Brain-derived and in vitro-seeded alpha-synuclein fibrils exhibit distinct biophysical profiles

Selene Seoyun Lee[1], **Livia Civitelli**[1*], **Laura Parkkinen**[1*]

***For correspondence:**
livia.civitelli@ndcn.ox.ac.uk;
laura.parkkinen@ndcn.ox.ac.uk

[1]Nuffield Department of Clinical Neurosciences, Oxford Parkinsons' Disease Center, University of Oxford, UK

Abstract The alpha-synuclein (αSyn) seeding amplification assay (SAA) that allows the generation of disease-specific in vitro seeded fibrils (SAA fibrils) is used as a research tool to study the connection between the structure of αSyn fibrils, cellular seeding/spreading, and the clinico-pathological manifestations of different synucleinopathies. However, structural differences between human brain-derived and SAA αSyn fibrils have been recently highlighted. Here, we characterize biophysical properties of the human brain-derived αSyn fibrils from the brains of patients with Parkinson's disease with and without dementia (PD, PDD), dementia with Lewy bodies (DLB), multiple system atrophy (MSA) and compare them to the 'model' SAA fibrils. We report that the brain-derived αSyn fibrils show distinct biochemical profiles, which were not replicated in the corresponding SAA fibrils. Furthermore, the brain-derived αSyn fibrils from all synucleinopathies displayed a mixture of 'straight' and 'twisted' microscopic structures. However, the PD, PDD, and DLB SAA fibrils had a 'straight' structure, whereas MSA SAA fibrils showed a 'twisted' structure. Finally, the brain-derived αSyn fibrils from all four synucleinopathies were phosphorylated (S129). However, the phosphorylation pattern was not maintained in the SAA fibrils, where only PDD and DLB SAA fibrils showed weak signs of phosphorylation. Our findings demonstrate the limitation of the SAA fibrils modelling the brain-derived αSyn fibrils and pay attention to the necessity of deepening the understanding of the SAA fibrillation methodology.

Introduction

Synucleinopathies are all characterized by abnormal accumulation of the protein alpha-synuclein (αSyn) in the brain. However, they are clinically and neuropathologically highly heterogeneous diseases with prominent disease-specific differences in presentation of symptoms, rate of disease progression, and the brain regions and cell types that are vulnerable to αSyn deposition and neuronal death. In Parkinson's disease (PD), Parkinson's disease with dementia (PDD), and dementia with Lewy bodies (DLB), αSyn aggregation is found in the neuronal soma as Lewy bodies (LBs) and in the axons and dendrites as Lewy neurites (LNs) (Figure **1**) (***Forno, 1988***; ***Spillantini et al., 1997***; ***Braak et al., 2003***). Furthermore, the astroglial accumulation of αSyn is a prominent but so far underdiagnosed pathology in these Lewy body disorders (***Altay et al., 2022***). The αSyn pathology in multiple system atrophy (MSA) is primarily found in oligodendrocytes as glial cytoplasmic inclusions (GCIs) (***Papp et al., 1989***).

The mechanistic link between αSyn and clinico-pathological diversity of the synucleinopathies is hypothesized to be the different fibrillar 'strains' of αSyn in analogy to prion disease. A strain is generated when αSyn monomers fold into specific fibrillar forms with distinct conformational and bio-

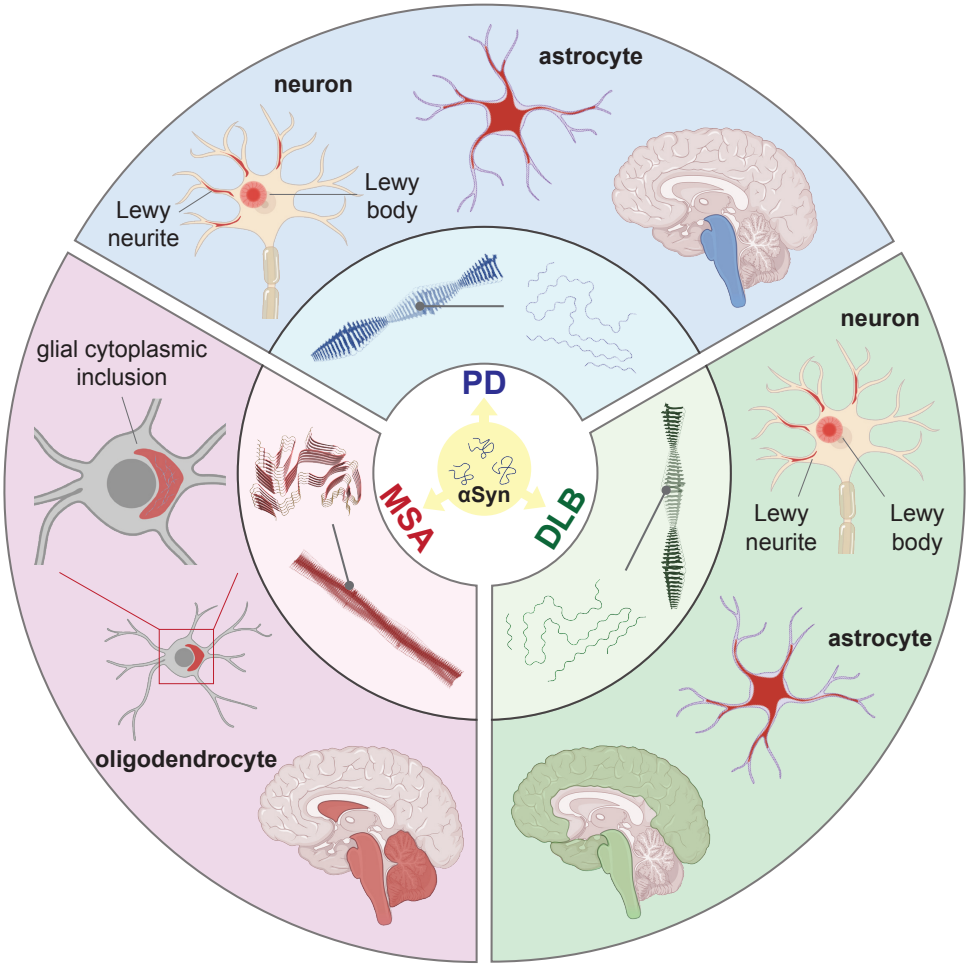

Figure 1. Distinct αSyn strains are associated with different neuropathological and clinical hallmarks of PD, DLB, and MSA. αSyn misfolds and aggregates into fibrils with characteristic conformations. At the atomic level, PD and DLB strains share a "Lewy fold" structure at the fibrillar core and comprise a single protofilament (***Yang et al., 2022***). MSA strains are twisted with two protofilaments intertwined, forming a different core structure to the "Lewy fold" (***Schweighauser et al., 2020***). At a cellular level, PD is characterized by significant neuronal loss at the brainstem, especially substantia nigra (SN), highlighted in blue. Lewy body (LB) and Lewy neurite (LN) accumulate in neurons. αSyn also accumulates in astrocytes, forming astroglial pathology. In DLB, the brainstem and neocortex are the most affected regions, highlighted in green. Here, LB and LN accumulate in neurons and astroglial pathology is also observed. In MSA, the cerebellum, basal ganglia and brainstem are the most affected, highlighted in red. Here, αSyn accumulates as glial cytoplasmic inclusions (GCIs) in the oligodendrocytes. The 3D structures of the αSyn fibrillar cores were generated using PyMOL, and the PDB structures from ***Schweighauser et al.*** (***2020***); ***Yang et al.*** (***2022***).

logical characteristics (***Melki, 2017***). Under the disease condition, misfolded and aggregated αSyn recruits normal, soluble endogenous αSyn to aggregate, and this self-perpetuating process spreads throughout the brain-periphery axis. Several studies have generated αSyn fibrils in vitro using various experimental conditions to characterize the presence of different strains (***Bousset et al., 2013***; ***Peelaerts et al., 2015***; ***Li et al., 2018***; ***Guerrero-Ferreira et al., 2019***; ***Lau et al., 2020***), but their relevance to human condition remains questionable. However, some studies have also examined αSyn fibrils extracted from the human brain tissue of different synucleinopathies and these have demonstrated that the human-derived αSyn strains exhibit distinct structures (***Schweighauser et al., 2020***), infectivity and bioactivity in cells (***Woerman et al., 2018a***, ***2019***; ***Ayers et al., 2022***) and animals (***Prusiner et al., 2015***; ***Lau et al., 2020***; ***Holec et al., 2022***; ***Peng et al., 2018***). The intrinsic structure of αSyn proteoforms may also depend on the local conditions of the brain region where they are formed and thus may vary within a single disease entity (***Peng et al., 2018***; ***Lau et al., 2020***; ***Schweighauser et al., 2020***). Future studies must comprehensively map the distinct fingerprints of human brain-derived αSyn strains to the disease.

Seeding amplification assays (SAAs) have become more applicable due to their feasibility in amplifying in vitro-seeded αSyn fibrils (SAA fibrils) from human biosamples. The SAA reaction incorporates a key characteristic of pathological αSyn, which is its ability to induce aggregation of monomeric αSyn into different complex conformers. This 'seeding' property is the critical mechanism of SAA. When pathological αSyn is present in the biosample, it seeds aggregation of the recombinant αSyn in the reaction, which is monitored in real-time using a fluorophore such as Thioflavin-T (ThT). SAA, together with different biosamples such as cerebrospinal fluid (CSF) (***Fairfoul et al., 2016***; ***Poggiolini et al., 2021***), brain homogenates (***Groveman et al., 2018***; ***Sano et al., 2018***), and skin punctures (***Mammana et al., 2020***; ***Kuzkina et al., 2021***), has presented its potential as a diagnostic method but also as a research tool to amplify disease-relevant fibrils. The newly amplified SAA fibrils are assumed to encode the intrinsic properties of the original seeding fibrils, thus being representative of the disease-specific strains. Therefore, using the 'model' SAA fibrils, studies have shown disease-specific structural, biochemical and phenotypic differences, suggesting the presence of distinct conformational αSyn strains in different synucleinopathies (***Strohaker et al., 2019***; ***Shahnawaz et al., 2020***; ***Van der Perren et al., 2020***; ***Frieg et al., 2022***). Recent studies have, however, demonstrated significant differences between the human brain-derived and SAA fibrils in their structure (***Lövestam et al., 2021***) and seeded pathology in vivo (***Van der Perren et al., 2020***). Nevertheless, there is currently a limited understanding of whether the resulting SAA fibrils truly preserve the original properties of the seeding fibrils across all the major synucleinopathies.

Here, we aim to investigate the biophysical differences between 1) the brain-derived αSyn fibrils in different synucleinopathies and 2) the brain-derived αSyn versus the corresponding SAA fibrils. We examine the brain-derived αSyn fibrils extracted from the brains of patients with PD, PDD, DLB, and MSA and the brain-derived versus SAA αSyn fibrils and show striking differences in their biochemical profile, structure, and phosphorylation pattern. Our findings reveal further evidence supporting the molecular diversity among αSyn fibrils from different synucleinopathies. Also, our study highlights the limitations of the SAA fibrils to fully mirror the brain-derived αSyn fibrils and the need to study further the mechanism of seeding amplification and the application of SAA fibrils.

Results

Detection of differential αSyn seeding activity from brain-derived fibrils of PD, PDD, DLB, and MSA

We extracted αSyn fibrils from the human brain of patients with PD (n = 3), PDD (n = 3), DLB (n = 3), MSA (n = 3) and healthy controls (n = 3) (Table S1). The entorhinal cortex was used for PD, PDD, and DLB, and the striatum for MSA, as these are one of the main affected regions with αSyn pathology in each disorder. The brain-derived fibrils were diluted 1: 1,000 and used as a seed in an SAA reaction

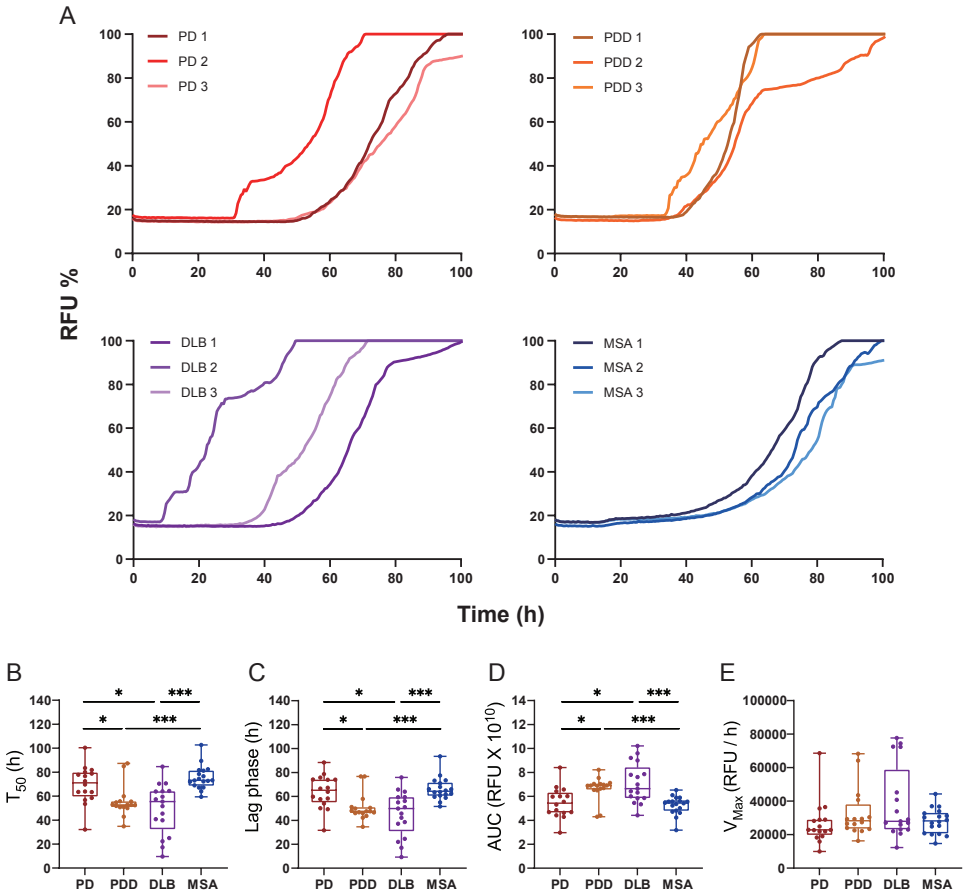

Figure 2. αSyn SAA seeded with αSyn fibrils from PD, PDD, DLB, and MSA brains. (**A**) SAA was performed with sarkosyl insoluble αSyn fibrils extracted from PD (n = 3), PDD (n = 3), DLB (n = 3), and MSA (n = 3) brains. The curves represent an average of six replicates. (**B**) Time to reach 50% of the maximum fluorescence (T_{50}). (**C**) The lag phase was taken at the time point where each positive reaction exceeded the threshold (RFU ≥ 5 SD). (**D**) Area under the curve (AUC). (**E**) The largest increase of fluorescence per unit of time (V_{MAX}). (**B-E**) Plotted values represent the six replicates of the three cases for each disease (N = 18). RFU, relative fluorescence unit; SD, standard deviation. *$P \leq 0.05$, **$P \leq 0.01$, ***$P \leq 0.005$

to generate in vitro amplified fibrils (SAA fibrils). PD, PDD, DLB, and MSA brain-derived αSyn fibrils reached the maximum ThT fluorescence within 100 h (Figure **2** A). The healthy controls did not display seeding potential (Figure **S1**), except for case 2 (HC 2), which showed an increasing signal towards the end of the reaction (approximately 91 h). The unseeded recombinant αSyn remained negative in all reactions. Kinetic parameters revealed a statistical difference in the seeding activities between PD/MSA and PDD/DLB. Kinetic parameters revealed a statistical difference in the seeding activities between PD/MSA and PDD/DLB. The time to reach 50 % of the maximum fluorescence (T_{50}) and the lag phase (time to reach five standard deviations of the minimum fluorescence) were significantly lower in PDD/DLB than in PD/MSA (Figure **2**B,C). As a result, the area under the curve (AUC) was statistically higher in PDD/DLB than in PD/MSA (Figure **2**D). However, the maximum rate of increase in fluorescence (V_{MAX}) was not statistically different among the diseases (Figure **2**E). Overall, the SAA kinetic parameters suggest PDD and DLB brain-derived αSyn fibrils have a more aggressive seeding capacity than PD and MSA.

Brain-derived and SAA αSyn fibrils display distinct biochemical profiles

At the end of the SAA reaction, the SAA αSyn fibrils were collected by ultracentrifugation. Having established that prion strains can be characterized by distinct biochemical profiles (***Lau et al., 2020***;

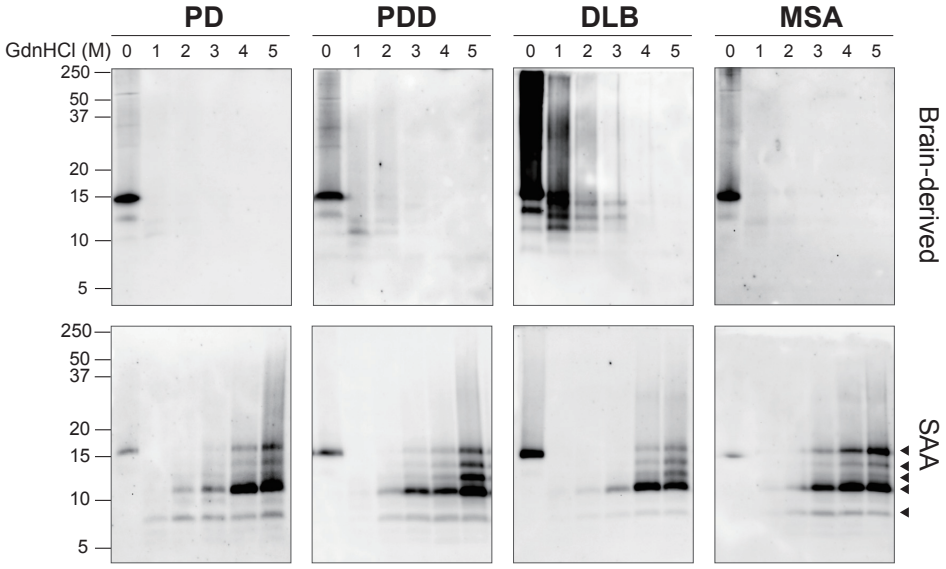

Figure 3. Brain-derived and SAA αSyn fibrils exhibited distinct biochemical profiles. Brain-derived and SAA αSyn fibrils were subjected to denaturation with increasing concentration of GdnHCl (0-5 M) and to PK digestion (1 µg/ml). The antibody clone 42 (BD Biosciences) was used to reveal the PK-resistant peptides. Immunoblots of one representative case from PD, PDD, DLB, and MSA are presented. The brain-derived and SAA fibrils are on the top and bottom rows, respectively. The molecular weights of the protein standards are shown in kilodaltons (kDa). Black arrows mark the five PK-resistant peptides revealed in the SAA fibrils. SAA, seeding amplification assay; GndHCl, guanidine-hydrochloride; PK, proteinase-K.

Shahnawaz et al., 2020; ***Sano et al., 2014***), we examined this characteristic in the brain-derived and SAA αSyn fibrils. First, the fibrils were denatured with increasing concentrations of guanidine hydrochloride (GdnHCl, 0-5 M) and then digested with proteinase-K (PK, 1 µg/ml).

The weakest GdnHCl (1 M) treatment completely denatured the PD and MSA brain-derived αSyn fibrils, as they were no longer visible on the immunoblot (Figure **3**). This result was consistent among all the three cases analyzed (Figure **S2**). Higher GdnHCl concentrations of 2 M and 3 M denatured PDD and DLB brain-derived αSyn fibrils, respectively (Figure **3**). The results illustrate that PD and MSA brain-derived αSyn fibrils have weaker biochemical stability than PDD and DLB fibrils.

The disappearance of the bands on the immunoblot after GndHCl treatment limited the comparative study of the αSyn fibrils between synucleinopathies. Therefore, we repeated the experiment using PK alone to improve the visualization of the biochemical profiles. The brain-derived αSyn fibrils were treated with five different PK concentrations starting from 0 mg/ml, incrementing to 1 mg/ml. PD cases contained mostly monomeric αSyn (15 kDa) that immediately degraded at the lowest PK concentration (1 ug/ml) (Figure **4**A). In contrast, in PDD, DLB, and MSA cases, high molecular weight (MW) bands above 15 kDa were observed, indicative of αSyn aggregates (Figure **4**B-D). Furthermore, lower MW bands (13, 10, 7 kDa) were also observed. As the PK concentration increased, the PDD and DLB fibrils gradually degraded, as the high MW bands started to disappear and low MW bands below 15 kDa began to appear (Figure **4**B,C). Similarly, the MSA fibrils gradually degraded as the PK concentration increased (Figure **4**D). However, low MW bands below 15 kDa were less prominent than those of PDD and DLB.

Although we experimented with an identical amount of total protein (10 ug), the amount of αSyn fibril could differ in each brain-derived sample. Using immunohistochemistry, we observed a lower load of αSyn pathology in PD and MSA brains than in PDD and DLB (Figure **S3**). In addition, the brain-derived fibrils were immunogold-labelled with anti-pαSyn and negatively stained for transmission electron microscopy (TEM). The samples were imaged with TEM at low magnification to observe

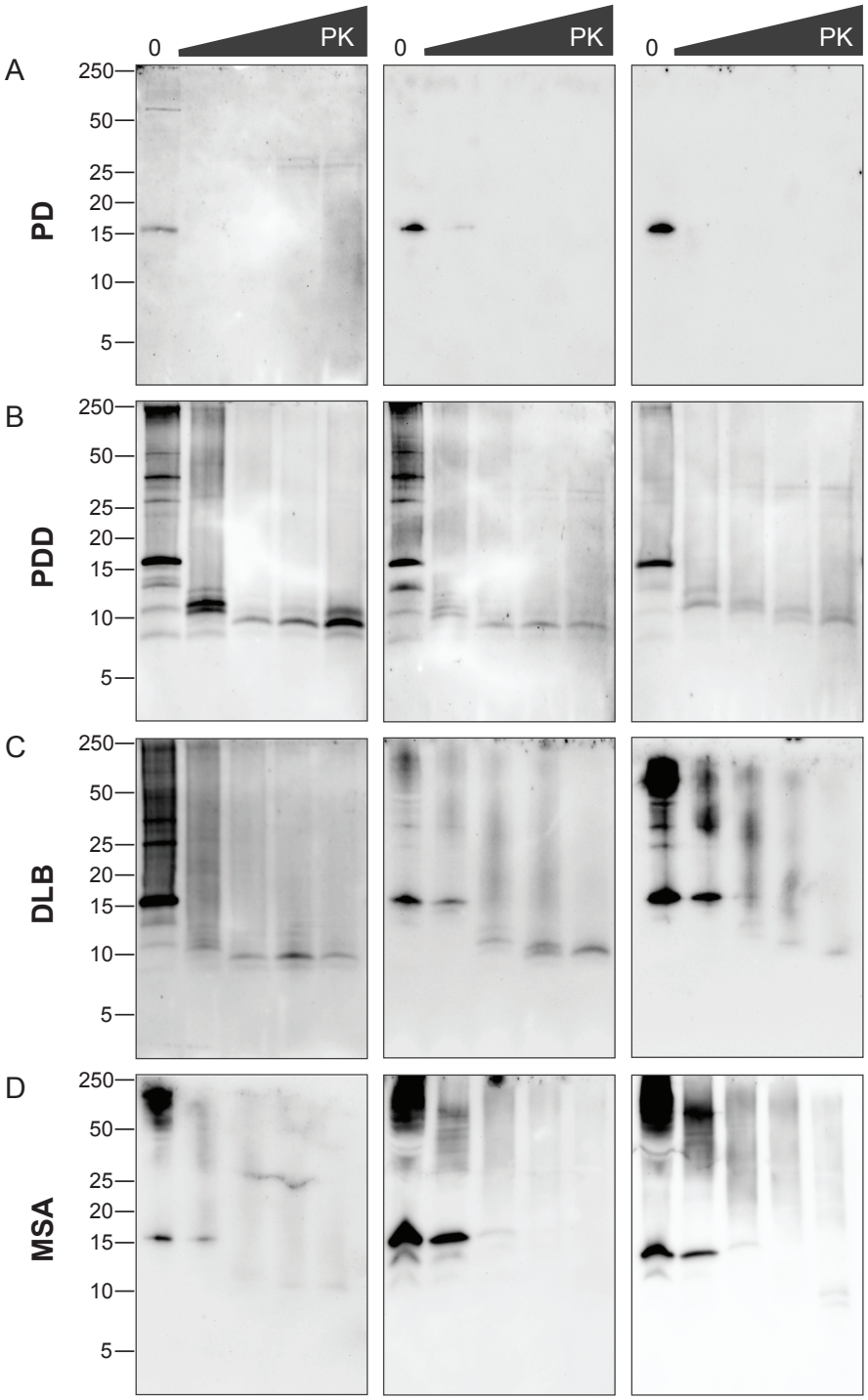

Figure 4. Proteinase-K degradation patterns of the brain-derived αSyn fibrils. The brain-derived αSyn fibrils from (**A**) PD, (**B**) PDD, (**C**) DLB, and (**D**) MSA were subjected to increasing concentrations of PK at 0, 0.001, 0.01, 0.1, and 1 mg/ml, represented by the escalating triangular bar. Western blot was performed using the antibody clone 42 (BD Biosciences). The molecular weights of the protein standards are shown in kilodaltons (kDa).

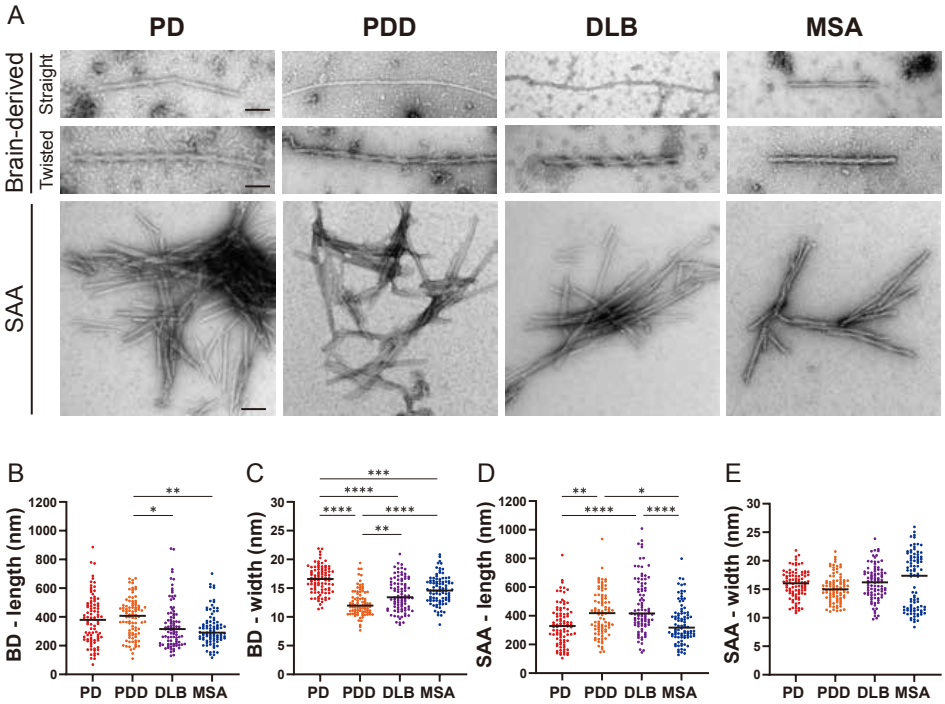

Figure 5. Transmission electron microscopy revealed different structures of brain-derived and SAA αSyn fibrils. (**A**) Electron microscope image of negatively stained brain-derived (BD) and SAA fibrils from PD, PDD, DLB, and MSA brains. (**B,C**) The lengths and widths of brain-derived fibrils. (**D,E**) The lengths and width of SAA fibrils. MSA SAA fibrils were twisted with alternating widths, resulting in two clusters of measurements. A total of 30 fibrils from each case were measured and plotted (N = 90). Scale bar = 50 nm. *$P \leq 0.05$, **$P \leq 0.01$, **** $P \leq 0.001$.

αSyn fibril density and distribution. PD and MSA cases contained 1-3 αSyn fibrils per region of interest (ROI), whereas PDD and DLB cases contained 3-5 αSyn fibrils per ROI (Figure **S4**). Adjacent slot blots also confirmed a higher amount of αSyn fibrils in PDD and DLB than in PD and MSA brain-derived samples. Therefore, lower fibril concentration in the PD and MSA brains could have limited the observation of the PK-resistant peptides using immunoblotting.

The SAA fibrils revealed markedly different biochemical profiles to the brain-derived αSyn fibrils. We observed identical profiles among all SAA fibrils from PD, PDD, DLB, and MSA. PK-resistant bands of 7 and 10 kDa started to appear after treatment with 2 M GdnHCl (Figure **3**). However, with increasing concentrations of GdnHCl, specific PK-resistant peptides appeared, consisting of five bands (7, 11, 12, 13, 14 kDa) (Figure **3**). These findings suggest that harsher denaturing conditions are required to destabilize the SAA fibrils and expose PK digestion sites. We concluded that SAA αSyn fibrils are more stable and characterized by distinct biochemical properties than the brain-derived αSyn fibrils.

Brain-derived and SAA αyn fibrils show structural differences

Next, we used TEM to investigate the structure of the brain-derived and SAA αSyn fibrils. The brain-derived αSyn fibrils from PD, PDD, and DLB exhibited two structures in TEM: straight and twisted (Figure **5**A, Figure **S5**). The fibrils from MSA were predominantly straight, with the rare presence of twisted type. Therefore, we only considered straight fibrils when comparing the dimensions of the fibrils among synucleinopathies. The length of the fibrils from different synucleinopathies ranged between 68 to 885 nm. Only the PDD fibrils were significantly longer than DLB and MSA (Figure **5**B). The width ranged from 7 to 21 nm, and there were significant differences between the diseases. PD had the widest fibrils, followed by MSA/DLB and PDD (Figure **5**C).

On the other hand, the SAA fibrils demonstrated a single dominant structure. PD, PDD, and DLB SAA fibrils were all straight, and MSA SAA fibrils were all twisted (Figure **5**A). Unlike the brain-derived fibrils, the SAA fibrils were highly clustered. The length of the SAA fibrils ranged from 104 to 1008 nm, and PDD/DLB SAA fibrils were significantly longer than those of PD/MSA (Figure **5**D). The width ranged from 8 to 25 nm, and the widths of the MSA SAA fibrils were distributed into two groups due to the alternating widths arising from the twisted structure. Unlike the brain-derived fibrils, the average widths of the SAA fibrils were similar between different synucleinopathies (Figure **5**E).

Overall, in DLB, the SAA fibrils were significantly longer and wider than the brain-derived fibrils (Figure **S6**). SAA fibrils from PDD were wider than the brain-derived fibrils but not different in length. The dimensions of the brain-derived and SAA fibrils from PD and MSA were not significantly different. However, it was difficult to compare the dimensions of the MSA fibrils as the brain-derived and SAA fibrils had different morphologies. Our observations demonstrate that brain-derived and SAA αSyn fibrils exhibit distinct TEM structures.

Brain-derived and SAA αSyn fibrils have distinct phosphorylation patterns

To confirm the identity of the fibrils imaged by TEM, we used immunogold with αSyn fibril conformation specific (MJFR-14) and pS129-specific (anti-pαSyn) antibodies. Both brain-derived and SAA fibrils from all four synucleinopathies were probed with MJFR-14, confirming that the fibrils were αSyn fibrils (Figure **6**A). The brain-derived fibrils were also strongly labeled with anti-pαSyn. MJFR-14 and anti-pαSyn, however, did not label the twisted brain-derived fibrils from PD, PDD, and DLB (Figure **6**B). The SAA fibrils from PD and MSA were not labeled with anti-pαSyn, but PD and MSA SAA fibrils were weakly labeled (Figure **6**A).

We performed a slot blot using identical antibodies to confirm the immunogold-labelling results. On the slot blot, DLB brain-derived αSyn fibrils showed the strongest signal with MJFR-14 and anti-pαSyn, followed by PDD, MSA, and PD (Figure **6**C). Interestingly, the anti-pαSyn signal from the SAA fibrils was markedly different from the brain-derived fibrils. In parallel to the anti-pαSyn immunogold results (Figure **6**A), PDD SAA fibrils showed the highest anti-pαSyn signal (Figure **6**D). The DLB SAA fibrils were also weakly phosphorylated, while those of PD and MSA were negative. Our results demonstrate that the brain-derived and SAA αSyn fibrils display different patterns of S129 phosphorylation.

Discussion

Strain-like properties of the brain-derived αSyn fibrils from different synucleinopathies.

Findings in this study provide evidence of distinct 'strain-like' properties of the brain-derived αSyn fibrils from different synucleinopathies. First, faster seeding kinetics was observed in the brain-derived αSyn fibrils from PDD and DLB than those from PD and MSA, suggesting a distinct 'strain' characterized by an aggressive seeding capacity. In contrast, those from PD and MSA are discrete 'strains' with milder seeding capacity. Previous studies of αSyn SAA with CSF showed that PD and MSA could be distinguished using T_{50}, V_{MAX} (***Poggiolini et al., 2021***), and F_{MAX} (***Shahnawaz et al., 2020***, ***2017***). However, in our αSyn SAA with brain-derived fibrils, the same parameters cannot distinguish between PD and MSA. Differences in the findings are likely to arise from the type of seeds. An unprocessed CSF would likely comprise distinct and different concentrations of αSyn species. Moreover, the choice of biosample (CSF, olfactory mucosa, skin) significantly affects the outcome of seeding kinetics (***Chahine et al., 2020***). By isolating the brain-derived αSyn fibrils, we could study the seeding kinetics of the fibrils themselves and, as a result, better understand their distinct intrinsic seeding properties.

Next, examining the phosphorylated brain-derived αSyn fibrils (pαSyn), we demonstrate a possible correlation between the amount of pαSyn and rapid seeding kinetics. Studies have shown

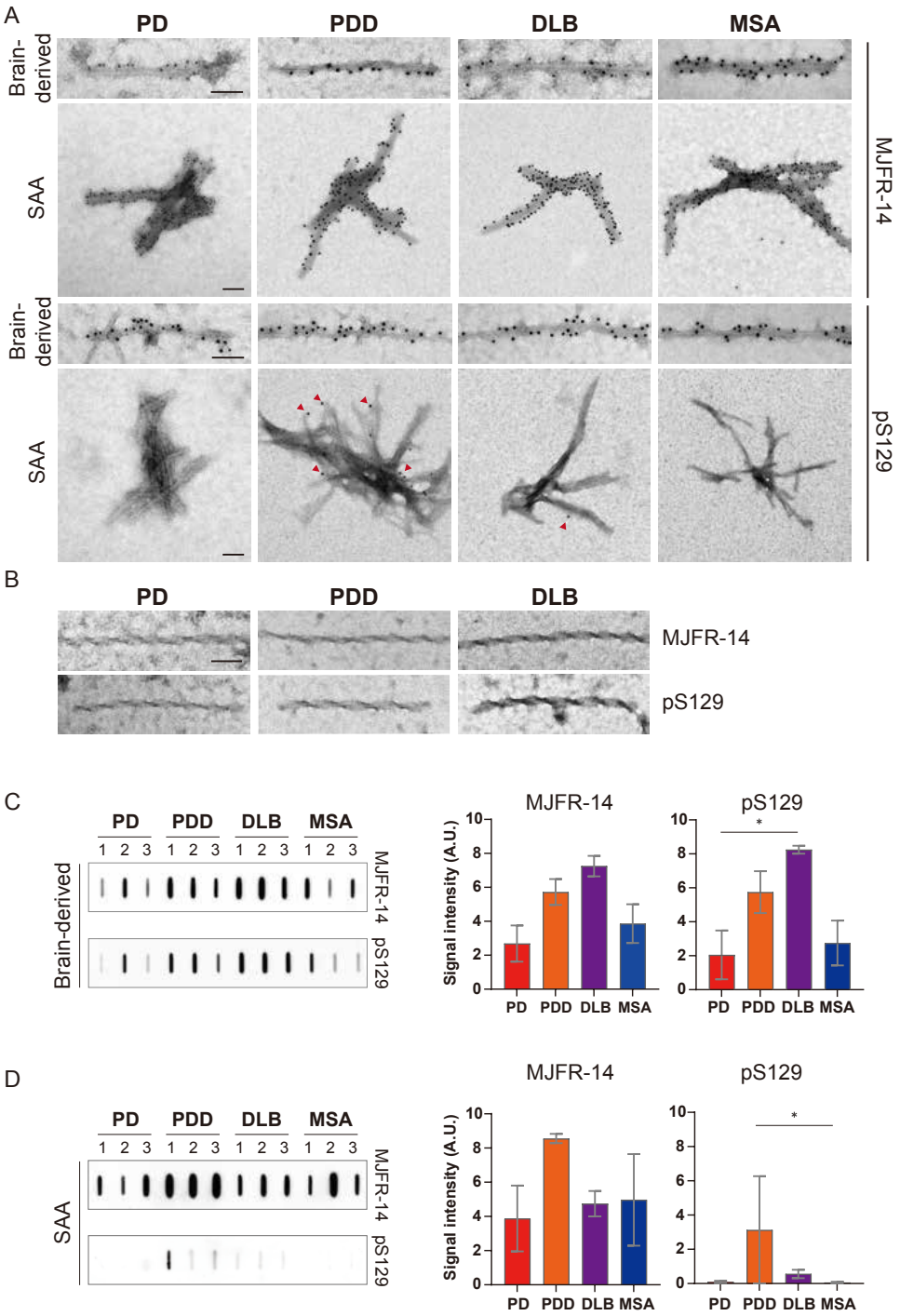

Figure 6. Brain-derived and SAA αSyn fibrils showed distinct phosphorylation patterns. (**A**) Electron microscope image of brain-derived and SAA αSyn fibrils from PD, PDD, DLB, and MSA brains labeled with fibril conformation-specific (MJFR-14) and anti-pαSyn (pS129) antibodies. (**B**) The twisted αSyn fibrils from PD, PDD, and DLB brains were not labeled for MJFR-14 and pS129. Scale bar = 50 nm. (**C,D**) Semi-quantification of αSyn fibrils and pαSyn confirm the different patterns of αSyn phosphorylation between brain-derived and SAA αSyn fibrils. The amount of αSyn fibrils and pαSyn in (**C**) brain-derived and (**D**) SAA fibrils was determined using a slot blot. Two µg of proteins were filtered on a nitrocellulose membrane and probed with MJFR-14 and pS129 antibodies. The semi-quantitative measurement was done by averaging the measurements of three cases from each disease. Error bars indicate ± one standard deviation (SD). * $P \leq 0.05$.

that pαSyn enhances αSyn aggregation in vitro (SH-SY5Y cells) and in vivo (rodent models) (***Smith et al., 2005***; ***Karampetsou et al., 2017***). However, contradicting findings have also been reported, suggesting a neuroprotective role of pαSyn (***Ma et al., 2016***; ***Ghanem et al., 2022***). Although the biological role of pαSyn is unclear, we report that a higher amount of pαSyn may contribute to the more aggressive seeding kinetics observed in PDD and DLB brain-derived αSyn fibrils than those of PD and MSA.

Further evidence of 'strain-like' property was exhibited by the distinct biochemical profiles of the brain-derived αSyn fibrils from different synucleinopathies. The brain-derived αSyn fibrils from PD and MSA were more susceptible to GndHCl denaturation than PDD and DLB, indicating conformational instability of PD and MSA brain-derived αSyn fibrils. Nevertheless, it must be noted that the rapid denaturation of PD fibrils might be due to a low concentration of αSyn fibrils, as demonstrated by a lower Lewy pathology load in the entorhinal cortex. A previous study also showed that human brain-derived αSyn fibrils from DLB were more stable than MSA by using GdnHCl treatment (***Lau et al., 2020***). Interestingly, the less stable MSA fibrils propagated faster in TgM83 mice than the more stable DLB fibrils. Such inverse correlation between conformational stability and disease propagation has been characterized in prion disease (***Legname et al., 2006***). Therefore, our findings on the differential conformational stability could reflect the strain-specific characteristics of αSyn fibrils. Subsequently, it could be related to the fast disease progression of MSA compared to PDD and DLB.

Subsequently, by assessing the PK-resistance of the αSyn fibrils, we illustrate further the molecular diversity of αSyn fibrils. The sizes of the low MW PK-resistant fragments differed between diseases and cases within each disease. These distinct PK-resistant peptides suggest the presence of conformational variants indicative of αSyn fibrillar strains within a single disease entity. Similarly, Guo and colleagues reported evidence of distinct αSyn fibrillar conformers in different PDD patients' brains (***Guo et al., 2013***). Our group has also shown different SAA kinetics in the CSF samples of PD patients divided into four different subtypes based on their baseline and progressive motor and non-motor symptoms (***Lawton et al., 2018***), suggesting αSyn strain heterogeneity within the same disease (***Poggiolini et al., 2021***). Finally, unlike PDD and DLB, MSA αSyn fibrils gradually disappeared upon PK treatment without being digested into small fragments. The lack of PK-resistant peptides in MSA indicates a readily digestible property of MSA αSyn fibrils. Together with its conformational instability, these biochemical properties might indicate a specific αSyn strain in MSA.

Interestingly, MSA fibrils also showed distinct structural features compared to those from PD, PDD, and DLB. The fibrils from MSA were predominantly 'straight', and those from PD, PDD, and DLB were 'straight' and 'twisted'. While the 'straight' brain-derived fibrils were densely decorated with MJFR-14 and anti-pαSyn antibodies, confirming their identity as a phosphorylated αSyn fibril, the 'twisted' fibrils were not recognised by these proteins. Similarly, Spillantini and colleagues also reported a finding of 'twisted' fibril from the cingulate cortex of a DLB brain with no labeling by the αSyn-specific antibody (***Spillantini et al., 1998***). Further ultrastructure analysis is essential to reveal the identity of the unlabeled twisted fibrils.

The methodological limitations of the structural characterisation in this study should be considered. Cryo-electron microscope (EM) ultrastructure revealed the twisted structures of the MSA brain-derived αSyn fibrils and single twisted protofilament structures in PD, PDD and DLB brains (***Yang et al., 2022***). Our TEM structures may differ due to the selection of different brain regions compared to those used in the literature and the limitation of the resolving power of TEM. Future cryo-EM structural studies of αSyn fibrils from not only different synucleinopathies but also different brain regions and subtypes of PD are required to establish a more profound understanding of the molecular diversity of the αSyn conformers in synucleinopathies.

Distinct biophysical properties between brain-derived and SAA fibrils.

In order to assess whether the SAA fibrils truly replicate the brain-derived fibrils (the seed), we compared the biophysical characteristics of the brain-derived αSyn fibrils and their respective SAA fibrils. First, by examining the resistance to GdnHCl and PK digestion, we illustrated a prominent biochemical difference between the brain-derived and SAA fibrils. High concentrations (4-5 M) of GdnHCl completely denatured the brain-derived fibrils, whilst SAA fibrils were still resistant. This indicates that the SAA fibrils are more stable and PK-resistant than their respective brain-derived fibrils. Furthermore, the SAA fibrils from all four synucleinopathies had identical patterns of PK resistance. The SAA amplifies fibrils with uniform biochemical features, losing the intrinsic properties of the original seed fibril and failing to replicate the biochemical properties of the original brain-derived fibrils.

The differences in biochemical stability might arise from the distinct distribution of the fibrils. SAA fibrils were clustered in negative-stain TEM, whereas the brain-derived fibrils were distributed in single filaments (Figure **5**). Also, this study used a PIPES-based buffer to amplify the SAA fibrils (***Poggiolini et al., 2021***). As the microenvironmental context of αSyn amplification substantially affects the newly amplified fibrils (***Peng et al., 2018***; ***Gustavsson et al., 2021***), the artificial in vitro environment can favor the formation of specific three-dimensional structures that are more conformationally stable.

Next, we showed that brain-derived fibrils display a mixture of straight and twisted structures, while SAA fibrils have a unified structure: straight (PD, PDD, DLB) or twisted (MSA). The striking structural difference may be due to a dominant seeding fibril within the mixture of brain-derived fibrils. Interestingly, straight fibrils were dominant in MSA brains, but the corresponding SAA fibrils were twisted. The commonality of a particular structure in a fibrillar mixture may not be a determinant of a dominant seeding fibril. Other factors might contribute, such as metal ions (***Uversky et al., 2001***) and post-translational modifications (PTMs), which also affect seeding efficiency (***Balana et al., 2023***). Also, our PIPES-based SAA reaction buffer with 150 mM NaCl is likely to have influenced the SAA fibril structure. However, the discrete structure of the MSA SAA fibrils compared to those of PD, PDD, and DLB implies that a complex matrix of intrinsic factors within the brain-derived fraction impacts seeding amplification and the resulting fibrillar structure.

A recent cryo-EM analysis of the MSA brain-derived and SAA fibrils revealed striking structural differences (***Schweighauser et al., 2020***; ***Lövestam et al., 2021***). A few significant differences included the protofilament fold, the inter-protofilament interface and the geometry of specific residues that shape the hydrophobic core. As the TEM has restricted resolution, future cryo-EM analyses are imperative to connect the structure to the disease heterogeneity and progression.

Lastly, we investigated the differences in the phosphorylation level between the brain-derived and SAA αSyn fibrils to identify differences in the PTM patterns. The brain-derived fibrils generally showed a higher phosphorylation level than the SAA fibrils. PDD and DLB SAA fibrils were weakly phosphorylated and decorated with pαSyn immunogold labels at the rare end of the fibrils (Figure **6**). Combining these findings, we can argue the possibility that the SAA fibrils extended from pαSyn species dissociated from the brain-derived fibrils. Therefore, the amount of initial pαSyn fibrils in the seed might be a critical determinant of the phosphorylation state of the resulting SAA fibrils.

Studies have explored the pathogenicity of brain-derived αSyn fibrils in vitro using primary neurons, oligodendrocytes, and HEK cell lines expressing mutated αSyn (***Woerman et al., 2018a***; ***Peng et al., 2018***; ***Woerman et al., 2015***; ***Yamasaki et al., 2019***). Moreover, similar pathological characterization has been done in different mouse models (***Lau et al., 2020***; ***Woerman et al., 2019***, ***2018a***; ***Prusiner et al., 2015***; ***Peng et al., 2018***; ***Masuda-Suzukake et al., 2013***; ***Watts et al., 2013***; ***Bernis et al., 2015***; ***Woerman et al., 2018b***, ***2020***). Interestingly, both in vitro and in vivo, MSA brain-derived αSyn induced significant αSyn aggregation, whereas those from PD/PDD and DLB brains produced either no or low αSyn accumulation. Similar disease-specific patterns were also observed in SAA-

amplified fibrils (***Shahnawaz et al., 2020***; ***Van der Perren et al., 2020***; ***Tanudjojo et al., 2021***). In future studies, it would be crucial to examine the brain-derived and SAA fibrils in comparison in cellular and mouse models for their pathological characteristics.

In summary, the distinct biochemical profiles and structures of the brain-derived αSyn fibrils from different synucleinopathies provide supporting evidence of molecular diversity of brain-derived αSyn fibrils among different synucleinopathies and individual patients. Moreover, the SAA fibrils failed to adopt the biochemical, structural and PTM properties of the seed brain-derived αSyn fibrils, which addresses a significant limitation of SAA in replicating the intrinsic biophysical properties of the seed fibrils. Therefore, our finding highlights the necessity of re-evaluating the SAA seeding mechanism and its capacity to generate disease-relevant αSyn fibrils used in different in vitro and in vivo models. Furthermore, it remains essential to investigate the human-derived αSyn fibrils in the different brain regions and in other peripheral sites to explore αSyn strains and how they may affect the progression of pathology. They also remain the most disease-specific fibrils used in cellular and animal models.

Methods and Materials

Patient Collection

Brain tissues from patients with PD and PDD were obtained from the Parkinson's UK Brain Bank (Imperial College London, UK) in accordance with approved protocols by the London Multicentre Research Ethics Committee. Brain tissues from patients with DLB, MSA and healthy controls were collected from the Oxford Brain Bank (OBB, University of Oxford, UK) in accordance with approved protocols by the South Central - Oxford C Research Ethics Committee (ref 23/SC/0241). All participants had given prior written informed consent for the brain donation. Both brain banks comply with the requirements of the Human Tissue Act 2004 and the Codes of Practice set by the Human Tissue Authority (HTA licence numbers 12275 for the Imperial and 12217 for OBB). The clinicopathological demographics of the patients and healthy controls are summarized in Table S1.

Extraction of αSyn fibrils from the human brain

Sarkosyl insoluble αSyn fibril was extracted from the brains of PD (n=3), PDD (n=3), DLB (n=3), MSA (n=3) patients and healthy controls (n=3). The entorhinal cortex was selected for PD, PDD, and DLB, and the striatum was selected for MSA. The extraction protocol was adapted from the method presented by Schweighauser and colleagues (***Schweighauser et al., 2020***). Brain tissues (0.5 g) were homogenized in an extraction buffer of 10 mM Tris-HCl, 0.8 M NaCl, 10% sucrose and 1 mM EGTA (pH 7.5). Sarkosyl was added to a final concentration of 2% and incubated for 30 min at 37 °C. Homogenates were centrifuged at 10,000 g for 10 min at 4 °C. The supernatants were centrifuged at 100,000 g for 60 min at 4 °C. The pellet was washed, resuspended in 500 µl/g of extraction buffer, and centrifuged at 500 g for 1 min at 4 °C. The resulting supernatants were diluted 1/3 in buffer consisting of 50 mM Tris-HCl, 0.15 M NaCl, 10 % sucrose, and 0.2% sarkosyl (pH 7.5). The diluted supernatant was centrifuged at 100,000 g for 60 min at 4 °C. The resulting pellet was washed and resuspended in 250 µl/g of 30 mM Tris-HCl (pH 7.5), being the sarkosyl-insoluble fraction. The protein concentration was determined using the bicinchoninic acid assay (BCA) (Thermo Scientific). The sarkosyl insoluble fraction was aliquoted and stored at -80 °C.

αSyn seeding amplification assay (SAA)

The brain-derived αSyn fibrils were diluted 1:1,000 in 30 mM Tris-HCl (pH 7.5), and 2 µl was added to 98 µl of the reaction mixture consisting of 100 mM PIPES (pH 7), 150 mM NaCl, 0.1 mg/ml of recombinant αSyn (rPeptide) and 10 µM thioflavin-T (ThT) to a final reaction volume of 100 µl. Before use, the recombinant αSyn was filtered through a 100 kDa molecular weight cut-off (MWCO) filter. The reaction mixture was loaded onto a black 96-well plate with a clear bottom (Nalgene Nunc). The plate was sealed with a plate sealing film (Thermo Scientific) and incubated at 42 °C

in a BMG FLUOstar Omega plate reader for 100 h with cycles of 1 min shaking (400 rpm double orbital) and 1 min rest. ThT fluorescence measurement (450 nm excitation and 480 nm emission) was taken every 30 min. Each sample was run in six replicates. The reaction end-products were ultracentrifuged at 100,000 g for 1 h at 4 °C and collected as SAA fibril.

Conformational stability assay and immunoblotting

The brain-derived αSyn fibrils (10 µg) and SAA fibrils (1 µg) were treated with different GdnHCl concentrations (0-5 M) at 37 °C for 1 h on a thermoshaker (800 rpm). The reactions were stopped by reducing the GdnHCl concentration to 0.5 M. The fibrils were treated with 1 µg/ml of proteinase-K (PK) at 37 °C for 30 min on a thermoshaker (500 rpm). Digested samples were collected using ultracentrifugation at 100,000 g, 4 °C for 1 h. Tricine sample buffer (Bio-Rad) was added to the samples and boiled at 95 °C for 10 min. The samples were analyzed with 16.5% Tris-Tricine gels (Bio-Rad) and immunoblotted on nitrocellulose membranes (Amersham). Membranes were blocked with 5% skimmed milk in TBS-Tween and incubated with anti-αSyn clone 42 (BD Biosciences, 1:1,000 dilution). In a slot blot, 2 µg of protein was immobilized on a nitrocellulose membrane (Amersham) by filtration using a slot blot apparatus (GE Healthcare). The membrane was blocked with 5% skimmed milk and probed with MJFR-14-6-4-2 (Abcam, 1:3000 dilution) and EP1536Y (Abcam, 1:1,000 dilution). The membranes were developed using an ECL Western blot detection kit (Amersham). Semi-quantitative analysis of the slot blot data was performed using ImageJ.

Transmission electron microscopy (TEM) and immunolabeling electron microscopy

Five µl of 0.5 µg brain-derived αSyn fibrils and 5 µl of SAA fibrils were applied to glow-discharged carbon grids (Agar Scientific, 300 mesh) and incubated for 2 min. The grid was washed with water for 10 sec and negatively stained with 2% uranyl acetate for 10 sec. Stained samples were imaged on an FEI Tecnai T12 microscope operated at 120 kV.

For immunolabeling, the fibrils were applied to glow-discharged carbon grids and blocked with a blocking buffer (0.2% fish gelatin in PBS). Then, the grid was incubated with antibodies targeting the phosphorylated αSyn (EP1536Y, Abcam, 1:20 dilution) and αSyn fibril conformer (MJFR-14-6-4-2, Abcam, 1:50 dilution). After washing with blocking buffer, the sample was incubated with goat anti-rabbit IgG coupled with 10 nm gold (Ab27234, Abcam) diluted 1:10 in the blocking buffer. Then, the grid was fixed with 0.1% glutaraldehyde in PBS. The samples were stained with 2% uranyl acetate for 30 s.

Immunohistochemistry

Six µm-thick sections of formalin-fixed paraffin-embedded (FFPE) human brain tissue sections were de-paraffinized in xylene (3 x 5 min) and rehydrated through decreasing concentration of industrial denatured alcohol (IDA) (100%, 100%, 90%, 70%; 5 min each) and subsequently in distilled water (5 min). For antigen retrieval, sections were treated with 70% formic acid for 15 min. The sections were then blocked with 3% H_2O_2 for 20 min and with 10% fetal bovine serum (FBS) in PBS for 30 min. Sections were incubated with anti-αSyn clone 42 (BD Biosciences) diluted 1:1,000 in 10% FBS overnight at 4 °C. After washing with PBS (3 x 5 min), sections were incubated with Ms/Rb-HRP secondary antibody (Agilent Technologies) for 30 min at RT. Sections were developed with Dako DAB (Agilent Technologies) and counterstained with haematoxylin. Finally, sections were mounted to coverslips with DPX (Thermo Scientific).

Statistical analysis

Mann-Whitney U test was used when comparing two independent groups. Independent Kruskal-Wallis Test was performed to compare more than three groups for SAA kinetic parameters Figure **2**, fibril dimensions (PD, PDD, DLB, and MSA) Figure **5**, and the amount of phosphorylated αSyn fibrils Figure **6**. P values < 0.05 were considered statistically significant. All statistical analyses were performed using SPSS Statistics, Version 28.

Acknowledgments

We thank all the patients and their families for the valuable brain donations for research. We also want to thank Dr. Errin Johnson and the Oxford bioimaging facility for providing access and training for transmission electron microscopy and assisting with acquiring the imaging data. We acknowledge Dr. Alan King Lun Liu for helping us with the case selection and analysis of the clinical summary of the patients. We acknowledge the Oxford Brain Bank, supported by Brains for Dementia Research (BDR) (Alzheimer Society and Alzheimer Research UK) and the National Institute for Health Research (NIHR) Oxford Biomedical Research Centre (BRC). LP is supported by the GSK-Institute of Molecular & Computational Medicine, NIHR Oxford BRC, Parkinson Foundation, the Michael J. Fox Foundation, the Galen and Hilary Weston Foundation, and the National Institute of Health. LC is supported by NIHR Oxford BRC.

Supplementary Material

Case	ID	Brain region	Sex	Duration (years)	Clinical diagnosis	Neuropathological Diagnosis	Braak αSyn stage	Braak tau stage	CERAD	Cause of death
PD 1	PD305	ECtx	M	8	PD	PD	6	2	C0	NA
PD 2	PD348	ECtx	M	6	PD	PD	6	2	C1	NA
PD 3	PD436	ECtx	M	8	PD	PD	6	2	C1	NA
PDD 1	PD125	ECtx	M	25	PDD	PDD	6	2	C2	NA
PDD 2	PD207	ECtx	M	10	PDD	PDD	6	2	C0	NA
PDD 3	PD295	ECtx	M	16	PDD	PDD	6	2	C1	NA
DLB 1	07/062	ECtx	M	<1	Possible AD	DLB+AD	6	3	C2	NA
DLB 2	08/134	ECtx	F	0	Possible AD	DLB+AD	6	3	C2	NA
DLB 3	01/172	ECtx	M	3	AD+CVD	DLB+AD	6	3	C2	NA
MSA 1	C1851	BG	M	5	PD	MSA	NA	NA	NA	Bronchopneumonia
MSA 2	14/118	BG	M	NA	MSA	MSA	NA	0	C0	NA
MSA 3	18/021	BG	F	2	MSA	MSA	NA	1	C0	NA
CTR 1	12/088	ECtx	M	NA	NA	Normal brain	NA	NA	NA	Coronary artery disease and chronic renal failure
CTR 2	12/161	ECtx	M	NA	NA	Normal brain	NA	NA	NA	Lung cancer
CTR 3	12/085	BG	F	NA	NA	Normal brain	NA	NA	NA	Necrotizing pancreatitis and atrial fibrillation

Table S1. Clinicopathological summary of the patients included in this study. The table summarizes the clinical and pathological reports of the patients included in this study. PD, Parkinson's disease; PDD, Parkinson's disease with dementia; DLB, dementia with Lewy body; MSA, multiple system atrophy; CTR, control; ECtx, entorhinal cortex; BG, basal ganglia; M, male; F, female; AD, Alzheimer's disease; CVD, cardiovascular disease; αSyn, α-synuclein.

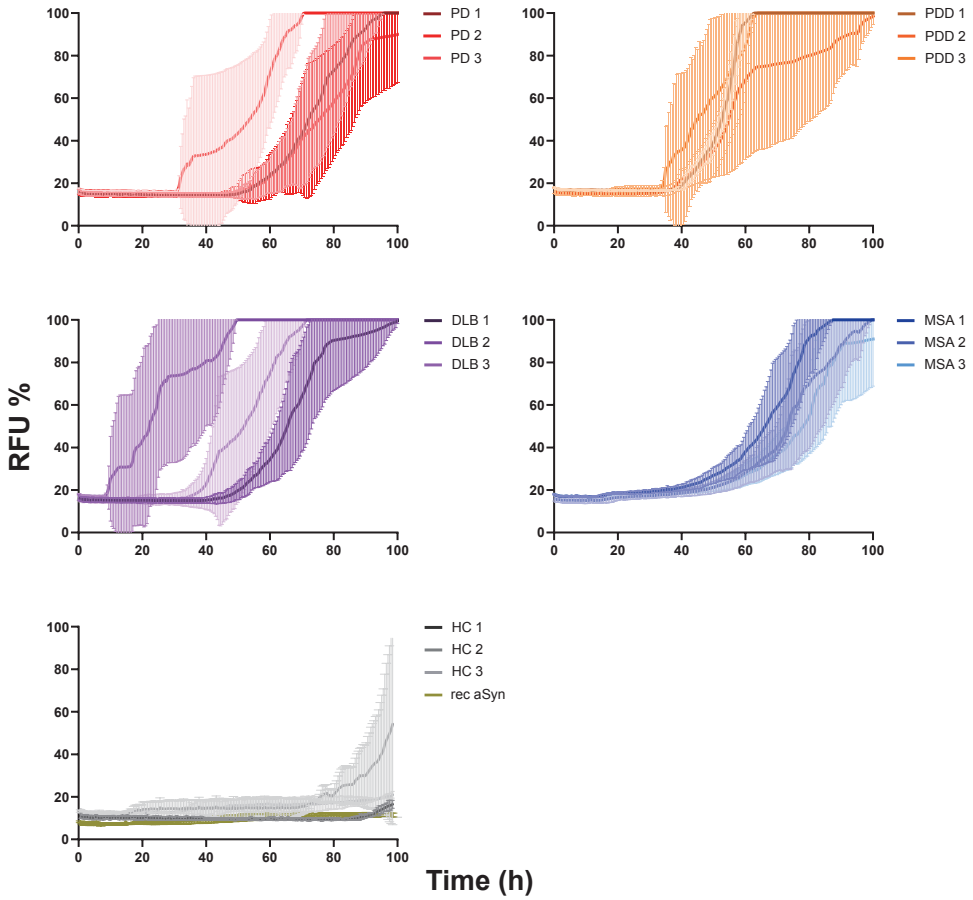

Figure S1. Raw data of the αSyn SAA reaction seeded with αSyn fibrils from PD, PDD, DLB, MSA, and healthy control brains. The curves represent the average of 6 replicates, and error bars indicate $\pm$ one standard deviation (SD). RFU, relative fluorescence unit.

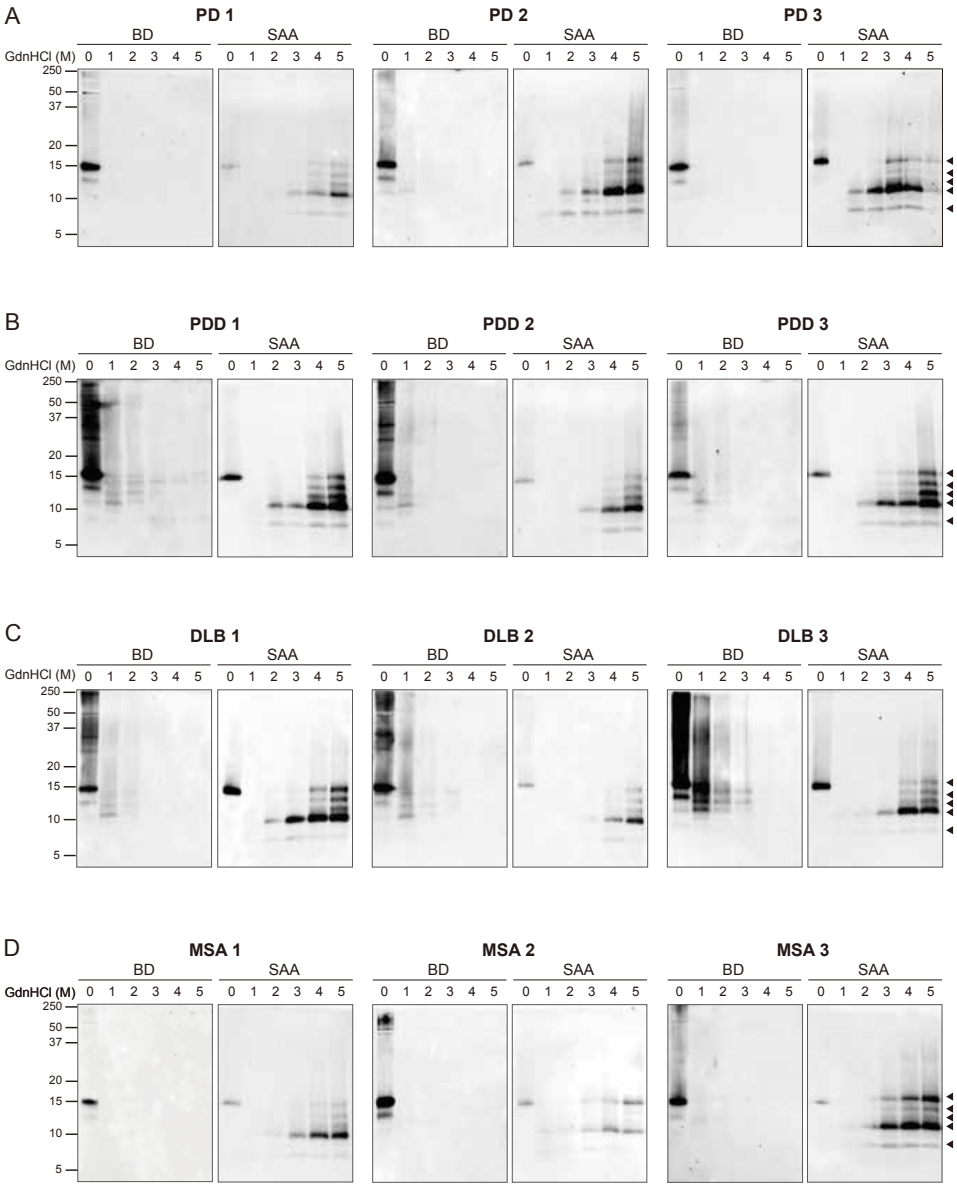

Figure S2. The full biochemical profiles of the brain-derived and SAA αSyn fibrils from all the cases. The brain-derived (BD) and SAA αSyn fibrils from all 3 cases of (**A**) PD, (**B**) PDD, (**C**) DLB, and (**D**) MSA were treated with GdnHCl (0-5 M) and PK (1 μ g/ml). The antibody clone 42 (BD Biosciences) was used to reveal the PK-resistant peptides. Black arrows mark the five PK-resistant peptides revealed in the SAA fibrils. The molecular weights of the protein standards are shown in kilodaltons (kDa). SAA, seeding amplification assay; GndHCl, guanidine-hydrochloride; PK, proteinase-K.

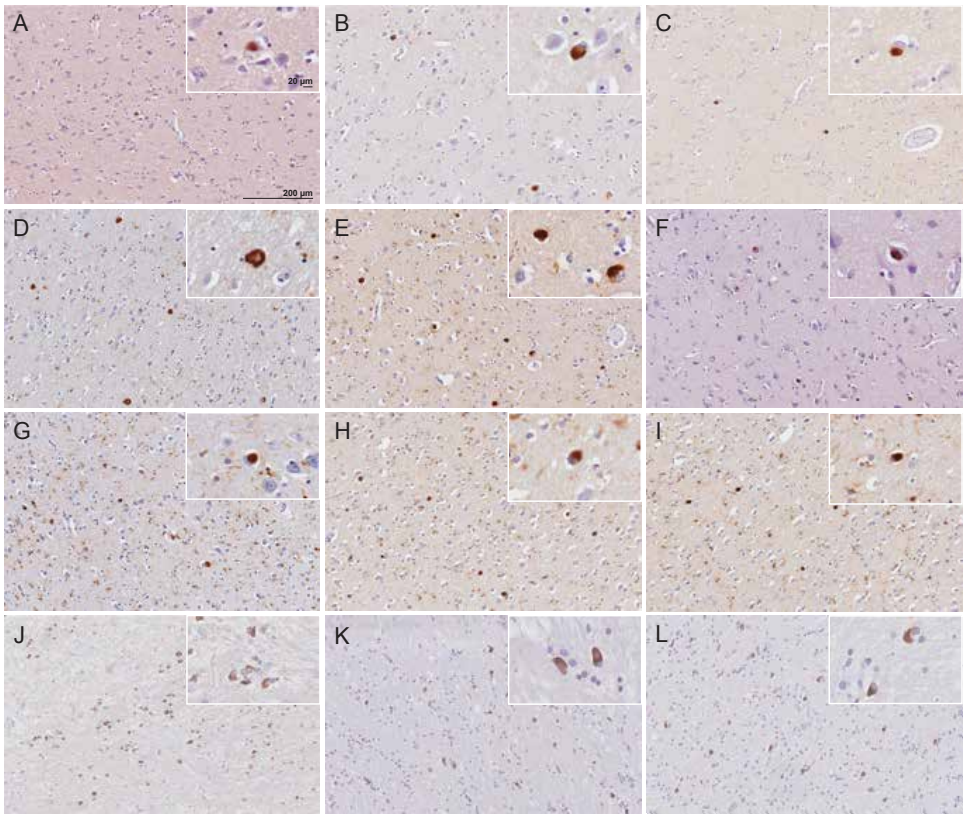

Figure S3. Immunohistochemical detection of αSyn in PD, PDD, DLB, and MSA brains. The entorhinal cortex (PD, PDD, DLB) and striatum (MSA) were stained with total αSyn using antibody clone 42 (BD Biosciences). (**A-C**) PD cases 1-3. (**D-F**) PDD cases 1-3. (**G-I**) DLB cases 1-3. (**J-L**) MSA cases 1-3. Scale bars = 20 µm and 200 µm.

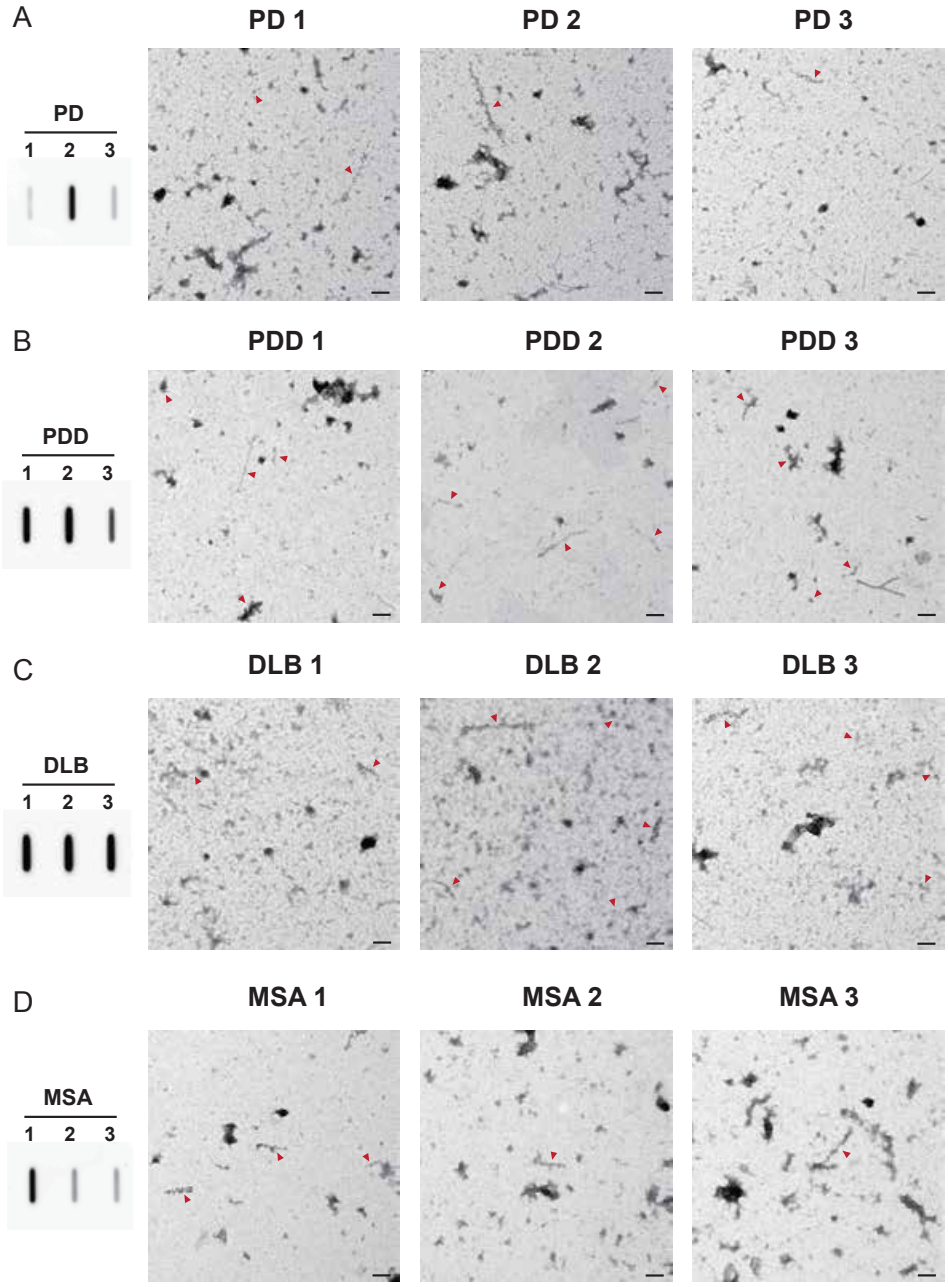

Figure S4. pS129 immunogold TEM images of the brain-derived αSyn fibrils. The brain-derived αSyn fibrils were labeled with anti-pαSyn (pS129) and imaged at low magnification to compare the relative quantities of the pαSyn fibrils between the diseases. All three cases were imaged for each disease (**A**) PD, (**B**) PDD, (**C**) DLB, and (**D**) MSA. The amount of pαSyn fibrils was examined using slot blots. Red arrows indicate labeled fibrils. Scale bar = 200 μm.

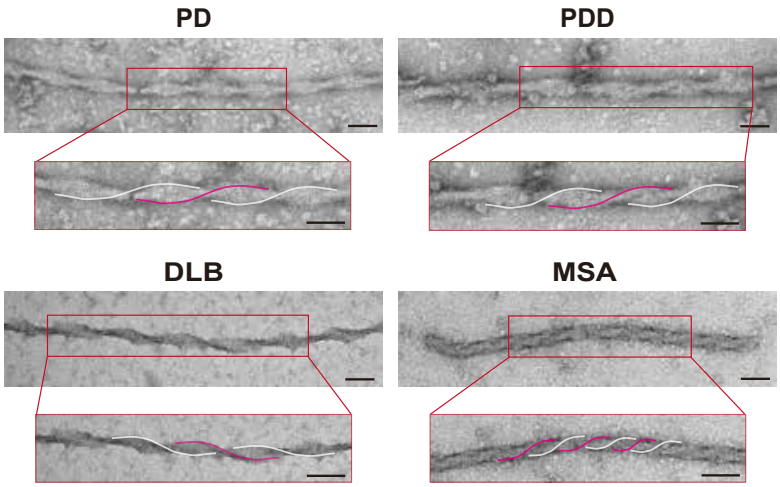

Figure S5. TEM images of the twisted brain-derived αSyn fibrils. PD, PDD, and MSA brain-derived fibrils displayed intertwined fibrils with left-handed helix and DLB brain-derived fibrils with right-handed helix. Helical twists are highlighted in pink and white. Scale bar = 50 μm.

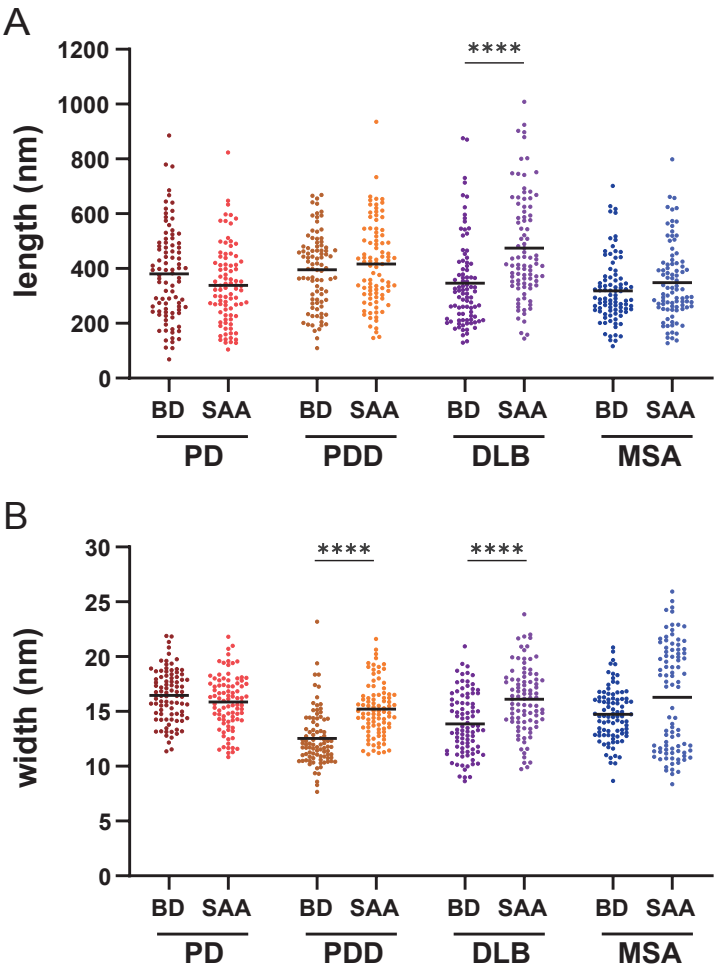

Figure S6. Comparison of the length and width of the brain-derived and SAA αSyn fibrils. Comparison of the (**A**) lengths and the (**B**) widths of the brain-derived and SAA αSyn fibrils. Thirty fibrils were counted for each case. Thus, a total of 90 data points were plotted (N = 90). The black bold line indicates an average. BD, brain-derived; SAA, seeding amplification assay. **** $P \leq 0.001$.

References

Altay, M. F., Liu, A. K. L., Holton, J. L., Parkkinen, L., and Lashuel, H. A. (2022). Prominent astrocytic alpha-synuclein pathology with unique post-translational modification signatures unveiled across lewy body disorders. *Acta Neuropathologica Communications*, 10(1):163.

Ayers, J. I., Lee, J., Monteiro, O., Woerman, A. L., Lazar, A. A., Condello, C., Paras, N. A., and Prusiner, S. B. (2022). Different α-synuclein prion strains cause dementia with lewy bodies and multiple system atrophy. *Proc Natl Acad Sci U S A*, 119(6).

Balana, A. T., Mahul-Mellier, A.-L., Nguyen, B. A., Horvath, M., Javed, A., Hard, E. R., Jasiqi, Y., Singh, P., Afrin, S., Pedretti, R., et al. (2023). O-glcnac modification forces the formation of an α-synuclein amyloid-strain with notably diminished seeding activity and pathology. *bioRxiv*, pages 2023–03.

Bernis, M. E., Babila, J. T., Breid, S., Wusten, K. A., Wullner, U., and Tamguney, G. (2015). Prion-like propagation of human brain-derived alpha-synuclein in transgenic mice expressing human wild-type alpha-synuclein. *Acta Neuropathol Commun*, 3:75.

Bousset, L., Pieri, L., Ruiz-Arlandis, G., Gath, J., Jensen, P. H., Habenstein, B., Madiona, K., Olieric, V., Bockmann, A., Meier, B. H., and Melki, R. (2013). Structural and functional characterization of two alpha-synuclein strains. *Nat Commun*, 4:2575.

Braak, H., Del Tredici, K., Rub, U., de Vos, R. A., Jansen Steur, E. N., and Braak, E. (2003). Staging of brain pathology related to sporadic parkinson's disease. *Neurobiol Aging*, 24(2):197–211.

Chahine, L. M., Beach, T. G., Brumm, M. C., Adler, C. H., Coffey, C. S., Mosovsky, S., Caspell-Garcia, C., Serrano, G. E., Munoz, D. G., III, C. L. W., Crary, J. F., Jennings, D., Taylor, P., Foroud, T., Arnedo, V., Kopil, C. M., Riley, L., Dave, K. D., Mollenhauer, B., and for the Systemic Synuclein Sampling Study (2020). In vivo distribution of α-synuclein in multiple tissues and biofluids in parkinson disease. *Neurology*, 95(9):e1267–e1284.

Fairfoul, G., McGuire, L. I., Pal, S., Ironside, J. W., Neumann, J., Christie, S., Joachim, C., Esiri, M., Evetts, S. G., Rolinski, M., Baig, F., Ruffmann, C., Wade-Martins, R., Hu, M. T., Parkkinen, L., and Green, A. J. (2016). Alpha-synuclein rt-quic in the csf of patients with alpha-synucleinopathies. *Ann Clin Transl Neurol*, 3(10):812–818.

Forno, L. S. (1988). The neuropathology of parkinson's disease. *Progress in Parkinson Research*, pages 11–21.

Frieg, B., Geraets, J. A., Strohäker, T., Dienemann, C., Mavroeidi, P., Jung, B. C., Kim, W. S., Lee, S.-J., Xilouri, M., Zweckstetter, M., and Schröder, G. F. (2022). Quaternary structure of patient-homogenate amplified α-synuclein fibrils modulates seeding of endogenous α-synuclein. *Communications Biology*, 5(1):1040.

Ghanem, S. S., Majbour, N. K., Vaikath, N. N., Ardah, M. T., Erskine, D., Jensen, N. M., Fayyad, M., Sudhakaran, I. P., Vasili, E., Melachroinou, K., et al. (2022). α-synuclein phosphorylation at serine 129 occurs after initial protein deposition and inhibits seeded fibril formation and toxicity. *Proceedings of the National Academy of Sciences*, 119(15):e2109617119.

Groveman, B. R., Orru, C. D., Hughson, A. G., Raymond, L. D., Zanusso, G., Ghetti, B., Campbell, K. J., Safar, J., Galasko, D., and Caughey, B. (2018). Rapid and ultra-sensitive quantitation of disease-associated alpha-synuclein seeds in brain and cerebrospinal fluid by alphasyn rt-quic. *Acta Neuropathol Commun*, 6(1):7.

Guerrero-Ferreira, R., Taylor, N. M., Arteni, A. A., Kumari, P., Mona, D., Ringler, P., Britschgi, M., Lauer, M. E., Makky, A., Verasdonck, J., Riek, R., Melki, R., Meier, B. H., Bockmann, A., Bousset, L., and Stahlberg, H. (2019). Two new polymorphic structures of human full-length alpha-synuclein fibrils solved by cryo-electron microscopy. *Elife*, 8.

Guo, J. L., Covell, D. J., Daniels, J. P., Iba, M., Stieber, A., Zhang, B., Riddle, D. M., Kwong, L. K., Xu, Y., Trojanowski, J. Q., and Lee, V. M. (2013). Distinct α-synuclein strains differentially promote tau inclusions in neurons. *Cell*, 154(1):103–17.

Gustavsson, N., Savchenko, E., Klementieva, O., and Roybon, L. (2021). The intracellular milieu of Parkinson's disease patient brain cells modulates alpha-synuclein protein aggregation. *Acta Neuropathologica Communications*, 9(1):1–6.

Holec, S. A. M., Lee, J., Oehler, A., Ooi, F. K., Mordes, D. A., Olson, S. H., Prusiner, S. B., and Woerman, A. L. (2022). Multiple system atrophy prions transmit neurological disease to mice expressing wild-type human α-synuclein. *Acta Neuropathol*, 144(4):677–690.

Karampetsou, M., Ardah, M. T., Semitekolou, M., Polissidis, A., Samiotaki, M., Kalomoiri, M., Majbour, N., Xanthou, G., El-Agnaf, O. M. A., and Vekrellis, K. (2017). Phosphorylated exogenous alpha-synuclein fibrils exacerbate pathology and induce neuronal dysfunction in mice. *Scientific Reports*, 7(1):16533.

Kuzkina, A., Bargar, C., Schmitt, D., Rößle, J., Wang, W., Schubert, A.-L., Tatsuoka, C., Gunzler, S. A., Zou, W.-Q., Volkmann, J., Sommer, C., Doppler, K., and Chen, S. G. (2021). Diagnostic value of skin rt-quic in parkinson's disease: a two-laboratory study. *npj Parkinson's Disease*, 7(1):99.

Lau, A., So, R. W. L., Lau, H. H. C., Sang, J. C., Ruiz-Riquelme, A., Fleck, S. C., Stuart, E., Menon, S., Visanji, N. P., Meisl, G., Faidi, R., Marano, M. M., Schmitt-Ulms, C., Wang, Z., Fraser, P. E., Tandon, A., Hyman, B. T., Wille, H., Ingelsson, M., Klenerman, D., and Watts, J. C. (2020). alpha-synuclein strains target distinct brain regions and cell types. *Nat Neurosci*, 23(1):21–31.

Lawton, M., Ben-Shlomo, Y., May, M. T., Baig, F., Barber, T. R., Klein, J. C., Swallow, D. M., Malek, N., Grosset, K. A., and Bajaj, N. (2018). Developing and validating parkinson's disease subtypes and their motor and cognitive progression. *Journal of Neurology, Neurosurgery & Psychiatry*, 89(12):1279–1287.

Legname, G., Nguyen, H.-O. B., Peretz, D., Cohen, F. E., DeArmond, S. J., and Prusiner, S. B. (2006). Continuum of prion protein structures enciphers a multitude of prion isolate-specified phenotypes. *Proceedings of the National Academy of Sciences*, 103(50):19105–19110.

Li, B., Ge, P., Murray, K. A., Sheth, P., Zhang, M., Nair, G., Sawaya, M. R., Shin, W. S., Boyer, D. R., Ye, S., Eisenberg, D. S., Zhou, Z. H., and Jiang, L. (2018). Cryo-em of full-length α-synuclein reveals fibril polymorphs with a common structural kernel. *Nat Commun*, 9(1):3609.

Lövestam, S., Schweighauser, M., Matsubara, T., Murayama, S., Tomita, T., Ando, T., Hasegawa, K., Yoshida, M., Tarutani, A., and Hasegawa, M. (2021). Seeded assembly in vitro does not replicate the structures of α-synuclein filaments from multiple system atrophy. *FEBS Open bio*, 11(4):999–1013.

Ma, M.-R., Hu, Z.-W., Zhao, Y.-F., Chen, Y.-X., and Li, Y.-M. (2016). Phosphorylation induces distinct alpha-synuclein strain formation. *Scientific Reports*, 6(1):37130.

Mammana, A., Baiardi, S., Rossi, M., Franceschini, A., Donadio, V., Capellari, S., Caughey, B., and Parchi, P. (2020). Detection of prions in skin punch biopsies of creutzfeldt-jakob disease patients. *Ann Clin Transl Neurol*, 7(4):559–564.

Masuda-Suzukake, M., Nonaka, T., Hosokawa, M., Oikawa, T., Arai, T., Akiyama, H., Mann, D. M., and Hasegawa, M. (2013). Prion-like spreading of pathological α-synuclein in brain. *Brain*, 136(Pt 4):1128–38.

Melki, R. (2017). How the shapes of seeds can influence pathology. *AA*.

Papp, M. I., Kahn, J. E., and Lantos, P. L. (1989). Glial cytoplasmic inclusions in the cns of patients with multiple system atrophy (striatonigral degeneration, olivopontocerebellar atrophy and shy-drager syndrome). *J Neurol Sci*, 94(1-3):79–100.

Peelaerts, W., Bousset, L., Van der Perren, A., Moskalyuk, A., Pulizzi, R., Giugliano, M., Van den Haute, C., Melki, R., and Baekelandt, V. (2015). alpha-synuclein strains cause distinct synucleinopathies after local and systemic administration. *Nature*, 522(7556):340–4.

Peng, C., Gathagan, R. J., Covell, D. J., Medellin, C., Stieber, A., Robinson, J. L., Zhang, B., Pitkin, R. M., Olufemi, M. F., Luk, K. C., Trojanowski, J. Q., and Lee, V. M. (2018). Cellular milieu imparts distinct pathological alpha-synuclein strains in alpha-synucleinopathies. *Nature*, 557(7706):558–563.

Poggiolini, I., Gupta, V., Lawton, M., Lee, S., El-Turabi, A., Querejeta-Coma, A., Trenkwalder, C., Sixel-Döring, F., Foubert-Samier, A., Le Traon, A. P., Plazzi, G., Biscarini, F., Montplaisir, J., Gagnon, J. F., Postuma, R. B., Antelmi, E., Meissner, W. G., Mollenhauer, B., Ben-Shlomo, Y., Hu, M. T., and Parkkinen, L. (2021). Diagnostic value of cerebrospinal fluid alpha-synuclein seed quantification in synucleinopathies. *Brain*.

Prusiner, S. B., Woerman, A. L., Mordes, D. A., Watts, J. C., Rampersaud, R., Berry, D. B., Patel, S., Oehler, A., Lowe, J. K., Kravitz, S. N., Geschwind, D. H., Glidden, D. V., Halliday, G. M., Middleton, L. T., Gentleman, S. M., Grinberg, L. T., and Giles, K. (2015). Evidence for α-synuclein prions causing multiple system atrophy in humans with parkinsonism. *Proc Natl Acad Sci U S A*, 112(38):E5308–17.

Sano, K., Atarashi, R., Ishibashi, D., Nakagaki, T., Satoh, K., and Nishida, N. (2014). Conformational properties of prion strains can be transmitted to recombinant prion protein fibrils in real-time quaking-induced conversion. *J Virol*, 88(20):11791–801.

Sano, K., Atarashi, R., Satoh, K., Ishibashi, D., Nakagaki, T., Iwasaki, Y., Yoshida, M., Murayama, S., Mishima, K., and Nishida, N. (2018). Prion-like seeding of misfolded α-synuclein in the brains of dementia with lewy body patients in rt-quic. *Mol Neurobiol*, 55(5):3916–3930.

Schweighauser, M., Shi, Y., Tarutani, A., Kametani, F., Murzin, A. G., Ghetti, B., Matsubara, T., Tomita, T., Ando, T., Hasegawa, K., Murayama, S., Yoshida, M., Hasegawa, M., Scheres, S. H. W., and Goedert, M. (2020). Structures of α-synuclein filaments from multiple system atrophy. *Nature*.

Shahnawaz, M., Mukherjee, A., Pritzkow, S., Mendez, N., Rabadia, P., Liu, X., Hu, B., Schmeichel, A., Singer, W., Wu, G., Tsai, A. L., Shirani, H., Nilsson, K. P. R., Low, P. A., and Soto, C. (2020). Discriminating alpha-synuclein strains in parkinson's disease and multiple system atrophy. *Nature*, 578(7794):273–277.

Shahnawaz, M., Tokuda, T., Waragai, M., Mendez, N., Ishii, R., Trenkwalder, C., Mollenhauer, B., and Soto, C. (2017). Development of a biochemical diagnosis of parkinson disease by detection of alpha-synuclein misfolded aggregates in cerebrospinal fluid. *JAMA Neurol*, 74(2):163–172.

Smith, W. W., Margolis, R. L., Li, X., Troncoso, J. C., Lee, M. K., Dawson, V. L., Dawson, T. M., Iwatsubo, T., and Ross, C. A. (2005). α-synuclein phosphorylation enhances eosinophilic cytoplasmic inclusion formation in sh-sy5y cells. *Journal of Neuroscience*, 25(23):5544–5552.

Spillantini, M. G., Crowther, R. A., Jakes, R., Hasegawa, M., and Goedert, M. (1998). alpha-synuclein in filamentous inclusions of lewy bodies from parkinson's disease and dementia with lewy bodies. *Proc Natl Acad Sci U S A*, 95(11):6469–73.

Spillantini, M. G., Schmidt, M. L., Lee, V. M., Trojanowski, J. Q., Jakes, R., and Goedert, M. (1997). Alpha-synuclein in lewy bodies. *Nature*, 388(6645):839–40.

Strohaker, T., Jung, B. C., Liou, S. H., Fernandez, C. O., Riedel, D., Becker, S., Halliday, G. M., Bennati, M., Kim, W. S., Lee, S. J., and Zweckstetter, M. (2019). Structural heterogeneity of alpha-synuclein fibrils amplified from patient brain extracts. *Nat Commun*, 10(1):5535.

Tanudjojo, B., Shaikh, S. S., Fenyi, A., Bousset, L., Agarwal, D., Marsh, J., Zois, C., Heman-Ackah, S., Fischer, R., Sims, D., Melki, R., and Tofaris, G. K. (2021). Phenotypic manifestation of α-synuclein strains derived from parkinson's disease and multiple system atrophy in human dopaminergic neurons. *Nature Communications*, 12(1):3817.

Uversky, V. N., Li, J., and Fink, A. L. (2001). Metal-triggered structural transformations, aggregation, and fibrillation of human α-synuclein: a possible molecular link between parkinson's disease and heavy metal exposure. *Journal of Biological Chemistry*, 276(47):44284–44296.

Van der Perren, A., Gelders, G., Fenyi, A., Bousset, L., Brito, F., Peelaerts, W., Van den Haute, C., Gentleman, S., Melki, R., and Baekelandt, V. (2020). The structural differences between patient-derived α-synuclein strains dictate characteristics of parkinson's disease, multiple system atrophy and dementia with lewy bodies. *Acta Neuropathol*, 139(6):977–1000.

Watts, J. C., Giles, K., Oehler, A., Middleton, L., Dexter, D. T., Gentleman, S. M., DeArmond, S. J., and Prusiner, S. B. (2013). Transmission of multiple system atrophy prions to transgenic mice. *Proc Natl Acad Sci U S A*, 110(48):19555–60.

Woerman, A. L., Kazmi, S. A., Patel, S., Aoyagi, A., Oehler, A., Widjaja, K., Mordes, D. A., Olson, S. H., and Prusiner, S. B. (2018a). Familial parkinson's point mutation abolishes multiple system atrophy prion replication. *Proceedings of the National Academy of Sciences*, 115(2):409–414.

Woerman, A. L., Kazmi, S. A., Patel, S., Freyman, Y., Oehler, A., Aoyagi, A., Mordes, D. A., Halliday, G. M., Middleton, L. T., Gentleman, S. M., Olson, S. H., and Prusiner, S. B. (2018b). Msa prions exhibit remarkable stability and resistance to inactivation. *Acta Neuropathologica*, 135(1):49–63.

Woerman, A. L., Oehler, A., Kazmi, S. A., Lee, J., Halliday, G. M., Middleton, L. T., Gentleman, S. M., Mordes, D. A., Spina, S., Grinberg, L. T., Olson, S. H., and Prusiner, S. B. (2019). Multiple system atrophy prions retain strain specificity after serial propagation in two different tg(snca*a53t) mouse lines. *Acta Neuropathologica*, 137(3):437–454.

Woerman, A. L., Patel, S., Kazmi, S. A., Oehler, A., Lee, J., Mordes, D. A., Olson, S. H., and Prusiner, S. B. (2020). Kinetics of α-synuclein prions preceding neuropathological inclusions in multiple system atrophy. *PLOS Pathogens*, 16(2):e1008222.

Woerman, A. L., Stöhr, J., Aoyagi, A., Rampersaud, R., Krejciova, Z., Watts, J. C., Ohyama, T., Patel, S., Widjaja, K., Oehler, A., Sanders, D. W., Diamond, M. I., Seeley, W. W., Middleton, L. T., Gentleman, S. M., Mordes, D. A., Südhof, T. C., Giles, K., and Prusiner, S. B. (2015). Propagation of prions causing synucleinopathies in cultured cells. *Proc Natl Acad Sci U S A*, 112(35):E4949–58.

Yamasaki, T. R., Holmes, B. B., Furman, J. L., Dhavale, D. D., Su, B. W., Song, E. S., Cairns, N. J., Kotzbauer, P. T., and Diamond, M. I. (2019). Parkinson's disease and multiple system atrophy have distinct α-synuclein seed characteristics. *J Biol Chem*, 294(3):1045–1058.

Yang, Y., Shi, Y., Schweighauser, M., Zhang, X., Kotecha, A., Murzin, A. G., Garringer, H. J., Cullinane, P. W., Saito, Y., Foroud, T., et al. (2022). Structures of α-synuclein filaments from human brains with lewy pathology. *Nature*, 610(7933):791–795.